

Article

Synthesis of Vinyl Chloride Monomer over Carbon-Supported Tris-(Triphenylphosphine) Ruthenium Dichloride Catalysts

Xing Li ^{1,2}, Haiyang Zhang ^{1,2,*} , Baochang Man ^{1,2}, Chuanming Zhang ^{1,2}, Hui Dai ³, Bin Dai ^{1,2} and Jinli Zhang ^{1,3,*}

¹ School of Chemistry and Chemical Engineering of Shihezi University, Shihezi 832000, Xinjiang, China; lixing19901015@163.com (X.L.); mbc13070097209@163.com (B.M.); zhchming163@163.com (C.Z.); db_tea@shzu.edu.cn (B.D.)

² Key Laboratory for Green Processing of Chemical Engineering of Xinjiang Bingtuan, Shihezi 832000, Xinjiang, China

³ School of Chemical Engineering & Technology, Tianjin University, Tianjin 300072, China; daihui028@tju.edu.cn

* Correspondence: zhy198722@163.com (H.Z.); zhangjinli@tju.edu.cn (J.Z.); Tel.: +86-993-2057-277 (H.Z.); +86-22-2789-0643 (J.Z.); Fax: +86-993-2057-210 (H.Z.); +86-22-2740-3389 (J.Z.)

Received: 24 May 2018; Accepted: 5 July 2018; Published: 9 July 2018



Abstract: A series of catalysts, including Ru/AC, *φ*-P-Ru/AC, *φ*-P-Ru/AC-HCl, and *φ*-P-Ru/AC-HNO₃, were prepared and evaluated for the hydrochlorination reaction of acetylene. The test results reveal that the *φ*-P-Ru/AC-HNO₃ catalyst shows superior catalytic performance with an initial acetylene conversion of 97.2% and a relative increment of 87.0% within 48 h in comparison with that of the traditional RuCl₃ catalyst. The substitution of inorganic RuCl₃ precursor by organic *φ*-P-Ru complex species in the catalysts results in more active species and tends to confine them in the micro-pores; the modification of carbon support by nitric acid in *φ*-P-Ru catalyst may produce an interaction between the functional groups on modified support and Ru species, which is favorable to anchor and then reduce the loss of active species during the reaction, further increasing the amount of dominating Ru species, and greatly improving the reactants adsorption ability on the catalysts, thus enhancing the performance of the resultant catalysts. The as-prepared *φ*-P-Ru catalysts are shown to be promising mercury-free candidates for the synthesis of vinyl chloride monomer.

Keywords: tris-(triphenylphosphine) ruthenium dichloride; acetylene hydrochlorination; mercury-free catalysts; enhanced interaction

1. Introduction

Currently, around 75% of vinyl chloride monomer (VCM) is produced in an area rich in coal resources by a direct process in which acetylene and hydrogen chloride are reacted with carbon-supported HgCl₂ as a catalyst. However, HgCl₂ is highly volatile and toxic, causing serious environmental pollution and personnel hazard. Therefore, the research and development of mercury-free catalyst is urgent, and scientists have put a lot of effort into finding alternative catalysts.

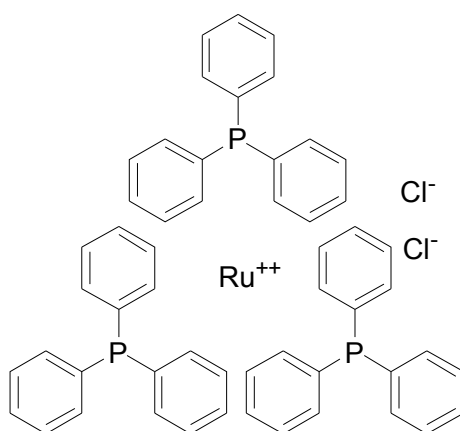
Hutchings was the first to show that carbon-supported Au catalysts have great potential for acetylene hydrochlorination. In his initial study the activity of metal catalysts is found to be related with the associated metal ions' standard electrode potentials [1] and AuCl₃ has a higher electrode potential. Subsequently, there was a great deal of research on gold catalysts [2–15]. However, Au-based catalysts do not have their advantages of economic performance because of the high price of Au. Therefore, it is essential to search a simple-prepared non-mercury catalyst for acetylene hydrochlorination, which is

characteristic of high activity, long-term stability and is more economic. According to the previous works by Hutchings, we found that RuCl_3 also has a higher electrode potential and it may be one of the probable alternatives. Zhu et al. calculated that the activation barrier via the DFT method for acetylene hydrochlorination, and found that the activation energy barrier is 9.1, 11.9 and 16.3 kcal/mol over RuCl_3 , AuCl_3 and HgCl_2 , respectively [16]. In our previous works, we found that the RuCl_3/SAC (SAC, spherical activated carbon) catalyst also had a good catalytic activity for acetylene hydrochlorination, but it needed to be improved; the catalyst RuCo(III)_3 exhibited a conversion more than 95% within 48 h, which was close to that of the Au catalysts with the same loading. To explore what Ru species accounted for a major role in the reaction, the RuCl_3/SAC catalyst was treated under different temperatures and atmospheres, and the results showed that the activity of catalyst was significantly increased after being treated; the presence of high valent ruthenium species was more beneficial to the hydrochlorination reaction of acetylene [17]. To further study the catalytic behavior of Ru-based catalysts, the effect of using carbon nanotubes as carriers and the addition of KCl on the catalytic performance were separately investigated; it was found that the confinement of Ru species in the electron-deficient inner tube and the addition of KCl can improve the dispersity of active species in the catalyst preparation process and promote the formation of more oxidation state ruthenium species, thus improving the catalytic activity [18]. Recently, we prepared the Ru-Co(III)-Cu(II) tri-metallic catalysts and revealed that the content of active components was low, and the dispersion was poor in Ru/SAC; it was easy to deactivate due to carbon deposition and the loss of active components; Cu(II) and Co(III) additives could synergistically make the most Ru exist in the form of high oxidation state ruthenium species, thus significantly improving the catalytic performance [19]. Gu et al. concluded that the loading of ammonium hexachlororuthenate precursor resulted in more active species and the catalyst performed higher activity for the hydrochlorination reaction of acetylene with an acetylene conversion of 90% when the reaction temperature was 170 °C, gas hourly space velocity (GHSV) of $\text{C}_2\text{H}_2 = 180 \text{ h}^{-1}$ and $V_{\text{HCl}}/V_{\text{C}_2\text{H}_2} = 1.1$ [20]. Shang et al. concluded that TPPB IL (tetraphenylphosphonium bromide ionic liquid) could improve the dispersion of ruthenium species, reduce the coking deposition on the catalysts, and suppress the reduction of Ru species, as a consequence, carbon-supported Ru@TPPB catalyst exhibited a superior performance with almost 100% conversion reached within 48 h [21]. In our recent work, it is unmasked that oxidation modification could generate an enhanced interaction between the support and active species, resulting in an improved performance over the modified Ru-O/AC-O (AC, activated carbon) catalyst [22].

The support for the catalysts also plays a key role in acetylene hydrochlorination. AC has the benefit of interactive functional groups on the surface and developed texture properties, suggesting that it may be a promising support for this reaction. In addition, modification of surface chemistry can also influence the catalytic behavior of catalyst. Wang et al. successfully synthesized an N-doped activated carbon catalyst and found that the N-doping could enhance the adsorption capacity of HCl on the catalyst, which is favorable for acetylene hydrochlorination [23]. Li et al. also synthesized an active Au catalyst via grafting the P-containing group on the support and found that modulation of P-dopants in AC was beneficial to interact with Au, resulting in an enhanced activity [3]. Liu et al. discussed the relationship between the catalytic activity/stability and the electronic properties, adsorption, and reducibility of the catalysts; they also addressed the modification strategies (e.g., heteroatom modification of support) and explorations of support/preparation method in their work, and these will enlighten the researchers to conduct the study on the modification of the support and active species [24].

According to the understanding of previous works: (i) The poor dispersion of Ru species is not favorable for acetylene hydrochlorination; (ii) The lower the content of the high-oxidation ruthenium species, the less active the catalyst. Hetero-atoms with lone pairs of electrons can stabilize Ru in the form of high-oxidation species, and the complexation of hetero-atomic groups with ruthenium species can also anchor and disperse the active species on the support. In this paper, the Ru catalysts were prepared with tri-(triphenylphosphine) ruthenium dichloride [$\text{RuCl}_2(\text{PPh}_3)_3$] (ϕ -P-Ru,

Scheme 1) supported on AC or acid-modified AC, and their catalytic performance was evaluated and characterized, aiming to explore an effective, economic, and easily prepared mercury-free catalyst.



Scheme 1. The molecular formula of tris-(triphenylphosphine) ruthenium(II) dichloride.

2. Results and Discussion

2.1. Results of the Catalytic Performance Test

Figure 1 shows the catalytic performance of different catalysts for hydrochlorination of acetylene. In our previous work, the supports exhibit relatively lower catalytic activity with 7.1%, 6.4%, and 5.7% acetylene conversions over bare AC, AC-HCl, and AC-HNO₃ catalysts, respectively (Figure S1) [25]. Under the same reaction conditions, there is a ca. 50% conversion reached over the original Ru/AC catalyst (Figure 1a). In comparison, the activity of ϕ -P-Ru/AC catalyst is greatly improved, and a 63.7% (yield of vinyl chloride = 63.3%) conversion is achieved within 48 h. The treatment of support by hydrochloric acid has a negligible effect on the catalytic performance of ϕ -P-Ru/AC catalyst. However, the modification of support by nitric acid is favorable for Ru-based catalysts to catalyze the synthesis of VCM, an initial conversion of 97.2% can be reached over ϕ -P-Ru/AC-HNO₃ catalyst, which decreases to 87.0% (yield of vinyl chloride = 86.6%) after 48 h reaction. The catalyst was also prepared by complexing aliphatic phosphine (P(Cy)₃, Cy, cyclohexyl) ligand with RuCl₃ precursor (Ru:P(Cy)₃ = 1:1, molar ratio) and the catalytic activity of the catalyst was assessed for acetylene hydrochlorination (Figure S2). It can be seen that a 51.8% conversion can be achieved over the Ru-P(Cy)₃/AC catalyst, lower than that of the ϕ -P-Ru/AC catalyst. In addition, the selectivity to VCM in all the catalysts exceeds 99.0% (Figure 1b). The above results indicate that the modification, especially by nitric acid, of support may generate an interaction between the support and ϕ -P-Ru species, significantly promoting the synthesized Ru catalysts' catalytic performance.

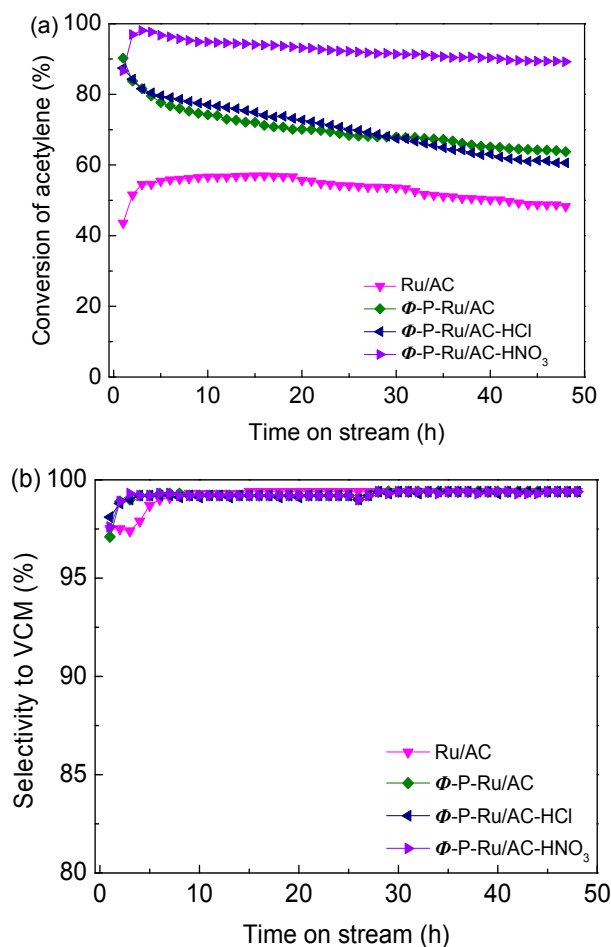


Figure 1. The acetylene conversion (a) and selectivity to VCM (b) over the synthesized catalysts. Reaction conditions: temperature (T) = 180 °C, GHSV (C₂H₂) = 180 h⁻¹ and V_{HCl}/V_{C₂H₂} = 1.15.

2.2. The Functional Groups on the Ru-Based Catalysts

To reflect the information of surface functional groups, FT-IR spectra of the different catalysts are recorded, and the results are presented in Figure 2. For the fresh bare AC (Figure S3), four characteristic bands centered at 1091, 1562, 2350, and 3400 cm⁻¹ appear, attributed to the absorption bands of C–OH, COOH, stretching vibration band of C≡N, and stretching vibration band of phenolic hydroxyl, respectively [26]. As mentioned in our previous work, compared with AC, the intensity of C=O, C–OH, and phenolic hydroxyl bands in AC-HCl catalyst is reduced, however, that of C≡N peak is increased after the modification. Meanwhile, the intensity of phenolic hydroxyl and C≡N bands in the AC-HNO₃ support is further reinforced, while that of C–OH peak is reduced, indicating the successful modification of functional groups on the support [25]. This may improve the surface hydrophilicity of the support to further improve the dispersity of the active species [22]. Compared with the bare support, the intensity of C≡N as well as the band of oxygen-containing functional groups on the original Ru/AC catalyst have been reduced to varying degrees. Apart from the characteristic bands that appear in the original Ru/AC catalyst, it also gives rise to the bands at 1080 cm⁻¹, 1450–1600 cm⁻¹ and 3030 cm⁻¹ in the ϕ -P-Ru/AC catalyst, attributed to the C–P stretching vibration band, C–C and C–H absorption vibration bands on the benzene ring, respectively [27]. This suggests the successful loading of ϕ -P-Ru on the carrier. For the ϕ -P-Ru/AC-HNO₃, the above characteristic bands are weakened; moreover, it is worth noting that the bands of some functional groups, especially the C≡N, are slightly shifted to higher values. These may also be due to the interaction between the modified functional groups on the treated support and ϕ -P-Ru species.

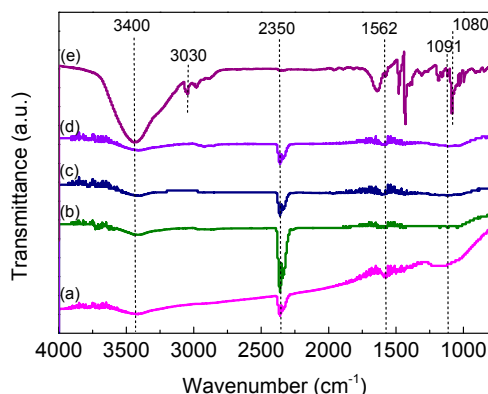


Figure 2. FT-IR spectra of: (a) Ru/AC; (b) ϕ -P-Ru/AC; (c) ϕ -P-Ru/AC-HCl; (d) ϕ -P-Ru/AC-HNO₃; (e) ϕ -P-Ru. The characteristic peaks are centered at: 1080 cm⁻¹: C–P; 1091 cm⁻¹: C–OH; 1562 cm⁻¹: COOH; 2350 cm⁻¹: C≡N; 3030 cm⁻¹: C–H; 3400 cm⁻¹: phenolic hydroxyl.

2.3. The Pore Properties of the Samples

The texture properties of all the related fresh and spent catalysts were revealed and listed in Table 1. The type-I adsorption isotherms for all of the catalysts suggests the micro-pores in the catalysts and the unchanged structure after the loading of Ru species (Figure S4) [28]. As can be seen from Table 1, the bare AC sample shows a maximum BET surface area (S_{BET}) of 1238 m²·g⁻¹ and total pore volume (V_{P}) of 0.69 cm³ g⁻¹. Both the S_{BET} s and V_{P} s of the supports change with the loading of RuCl₃ or Ru complex species. It is not difficult to find that the loading of the Ru species significantly decreases the S_{BET} s and V_{P} s, which ascribes to the so-called dilution effect [6]. The active species fill or block some of the support pores, leading to a decrease of the BET surface areas and total pore volumes, and the proportion of the support is reduced with the loading of the active components. However, the effects of the inorganic Ru and organometallic complex precursors on the textural properties are not the same (Table 1). For the Ru/AC catalyst, the loading of the active RuCl₃ species appears to decrease external surface area indicated by the decrease in the $S_{\text{ext.}}$ and $V_{\text{ext.}}$ and the almost unchanged $S_{\text{micro.}}$, $V_{\text{micro.}}$ and average pore diameter (D_{p}), which results from the loading of active species on the support's surface. In comparison, it is clearly that the loading of organometallic ϕ -P-Ru complex also significantly affects the S_{BET} and pore property of ϕ -P-Ru/AC catalyst. After loading of ϕ -P-Ru species, the S_{BET} and V_{P} of ϕ -P-Ru/AC catalyst decrease to 957 m² g⁻¹ and 0.53 cm³ g⁻¹, respectively. But the difference is that the loading of organometallic complex (ϕ -P-Ru) seems to significantly decrease micro-pore surface area and pore volume indicated by the obvious decrease in the $S_{\text{micro.}}$ and $V_{\text{micro.}}$ and an increase in D_{p} , which indicates that the active species tend to be loaded into micro-pores. Compared with ϕ -P-Ru/AC, the treatment of AC by hydrochloric acid slightly increases the active species anchored in the external surface, and there is almost no change after modification of AC by nitric acid. The spent catalysts exhibit lower S_{BET} s and V_{P} s than those of the related fresh ones. Through the data analysis, it can be seen that the relative differences of the fresh and spent catalysts' S_{BET} s ($\Delta S_{\text{BET}}\%$) and V_{P} s ($\Delta V_{\text{P}}\%$) decrease in the following order: ϕ -P-Ru/AC-HNO₃ > ϕ -P-Ru/AC-HCl > ϕ -P-Ru/AC > Ru/AC > AC. The significant increase of $\Delta S_{\text{BET}}\%$ and $\Delta V_{\text{P}}\%$ of the Ru-based catalysts compared with those of bare AC may be attributed to the metal-catalyzed reaction [29]. The decline of S_{BET} and V_{P} could attribute to the carbon deposition resulted from the polymerization of acetylene or vinyl chloride monomer at high temperature or the collapse of the pores during the reaction, leading to the decrease in the catalysts' activity [28]. The substitution of inorganic RuCl₃ precursor with organometallic ϕ -P-Ru complex is beneficial to anchor and further reduce the loss of the active species in the micro-pores, which can be verified according to the ICP-AES results (Table S1). The acid modification of carrier in the ϕ -P-Ru catalysts may result in serious carbonaceous material deposition or collapse of the pores during the reaction, which can also be indirectly confirmed by the increase of D_{p} after the reaction.

Table 1. Physical properties of the different Ru-based samples.

Samples	S_{BET}^a ($\text{m}^2 \text{g}^{-1}$)	ΔS_{BET} (%)	$S_{\text{micro.}}^b$ ($\text{m}^2 \text{g}^{-1}$)	$S_{\text{ext.}}^c$ ($\text{m}^2 \text{g}^{-1}$)	V_{P}^d ($\text{cm}^3 \text{g}^{-1}$)	ΔV_{P} (%)	$V_{\text{micro.}}^e$ ($\text{cm}^3 \text{g}^{-1}$)	$V_{\text{ext.}}$ ($\text{cm}^3 \text{g}^{-1}$)	D_{pore}^f (nm)
Fresh AC	1238	25.1	704	534	0.69	27.5	0.39	0.30	2.22
Used AC	927		514	413	0.50		0.29	0.21	2.17
Fresh Ru/AC	1160	31.7	698	462	0.64	31.3	0.39	0.25	2.22
Spent Ru/AC	792		401	391	0.44		0.23	0.21	2.22
Fresh ϕ -P-Ru/AC	957	34.2	496	461	0.53	32.1	0.28	0.25	2.23
Spent ϕ -P-Ru/AC	630		255	375	0.36		0.15	0.21	2.26
Fresh ϕ -P-Ru/AC-HCl	845	51.9	462	382	0.47	51.1	0.26	0.21	2.20
Spent ϕ -P-Ru/AC-HCl	406		143	263	0.23		0.09	0.14	2.23
Fresh ϕ -P-Ru/AC-HNO ₃	927	56.6	478	449	0.52	55.8	0.27	0.25	2.24
Spent ϕ -P-Ru/AC-HNO ₃	402		144	258	0.23		0.09	0.14	2.27

^a S_{BET} : BET specific surface area; ^b t-plot micropore area; ^c t-plot external surface area; ^d V_{P} : total pore volume, Volume at $p/p_0 = 0.98$; ^e t-plot micropore volume; ^f Adsorption average pore width ($4V/A$ by BET).

2.4. The Coking Deposition on the Catalysts

The obtained TG and DTG curves of the ϕ -P-Ru/AC-HNO₃ catalysts before and after the reaction are presented in Figure 3. Neither the fresh nor the spent catalyst exhibits an obvious weight loss when the temperature is lower than 150 °C, resulting from the negligible small molecules or water desorption in the catalysts [30]. The prominent weight loss appears in the range of 150–410 °C, reflecting the coking deposition on the ϕ -P-Ru/AC-HNO₃ catalyst. A rapid weight loss for both the catalysts takes place above 410 °C because of the burning of the activated carbon carrier under an air atmosphere. Based on the above analysis, the amount of coking deposition should be calculated by the difference of weight loss in the catalysts before and after reaction within the range of 150–410 °C [31].

Accordingly, the calculated amounts of coking deposition on all the catalysts are listed in Table 2. It decreases in the following order: ϕ -P-Ru/AC-HNO₃ > ϕ -P-Ru/AC-HCl > ϕ -P-Ru/AC > Ru/AC (Figure S5). The results are in accord with the measured results of texture parameters presented in Table 1. The substitution of the inorganic RuCl₃ precursor with ϕ -P-Ru does not inhibit the occurrence of carbon deposition, moreover, the treatment of the support by acid, especially by nitric acid, leads to more serious carbon deposition instead.

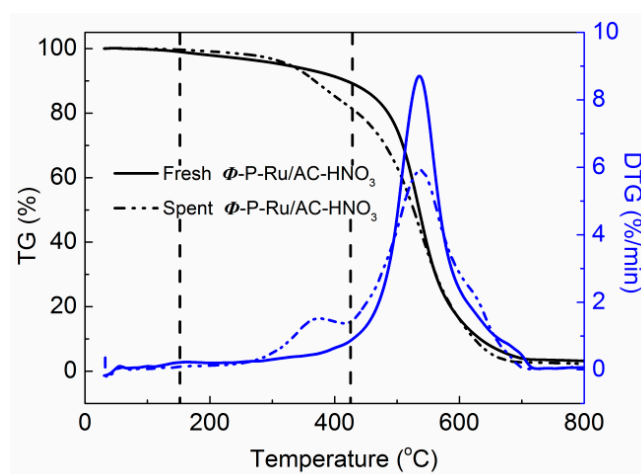


Figure 3. TG curves of the fresh and spent ϕ -P-Ru/AC-HNO₃ catalysts.

Table 2. The amount of coke deposition on the spent Ru-based catalysts.

Catalysts	Amount of Carbon Deposition (%)
Ru/AC	2.8 [25]
ϕ -P-Ru/AC	3.9
ϕ -P-Ru/AC-HCl	4.1
ϕ -P-Ru/AC-HNO ₃	7.2

2.5. The Dispersity of Ru Species on the Catalysts

Figure 4 shows XRD patterns of the catalysts, including the bare AC, original Ru/AC, ϕ -P-Ru/AC, ϕ -P-Ru/AC-HCl and ϕ -P-Ru/AC-HNO₃. No characteristic Ru reflections are detected apart from the amorphous diffraction reflections of carbon (Figure 4a), which indicates that Ru species are highly dispersed in the support and the size is smaller than the XRD detection limit, or the active centers are exist in the amorphous form in the catalysts [25,32]. For the spent catalysts, there still no discernible Ru reflections are observed in the XRD patterns (Figure 4b), indicating that the active components are not obviously agglomerated or sintered in the reaction. To further observe the size change of the active particles, TEM images of the catalysts are also obtained (Figure S6). It can be seen that the

active species are difficult to distinguish, predicting the good dispersity of them on the catalysts or the amorphous form of the active species, in accord with the XRD analysis.

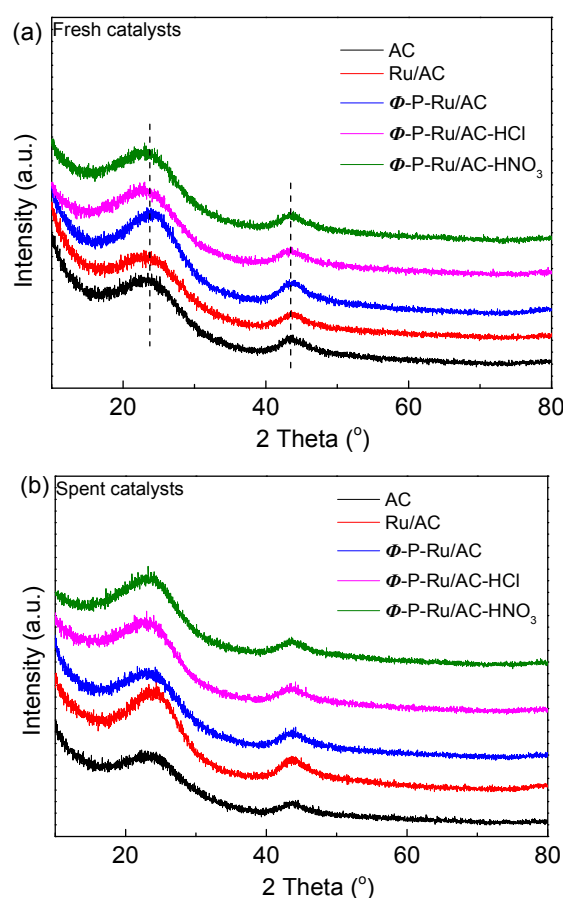


Figure 4. XRD patterns of the fresh (a) and spent (b) Ru-based catalysts.

2.6. Valence Change of Ru Species in the Synthesized Catalysts

Figure 5 shows the H₂-TPR profiles of the synthesized catalysts. The broad peak appeared in the range of 400–800 °C in fresh bare AC relates with the methanation of functional groups (Figure 5a) [18,33]. As mentioned in our previous work, it can be seen that there appear three reduction peaks located at ca. 150.3, 257.0, and 324.8 °C in the profile of fresh Ru/AC catalyst, corresponding to the reduction of RuO_x ($x > 2$), RuO₂, and RuCl₃, respectively [25]. The reduction temperatures in ϕ -P-Ru/AC catalyst shift to ca. 192.6 °C for RuO_x, 225.4 °C for RuO₂, and 291.7 °C for RuCl₃, respectively. The ϕ -P-Ru/AC-HCl and ϕ -P-Ru/AC-HNO₃ catalysts exhibit the curves similar to that of the untreated catalyst ϕ -P-Ru/AC, with temperatures shift to the higher values. Moreover, compared with those of the original Ru/AC catalyst, these reduction peaks of Ru species in ϕ -P-Ru catalysts are connected with the reduction peaks of functional groups on activated carbon support, forming broad shoulder peaks. The temperature shifts and the formed broad shoulder peaks indicate the enhanced interactions between the modified functional groups on the support and Ru species, which in turn affects the anchoring of Ru species (Table S1) and the relative content of them. Through comparing the TCD signals with a standard (CuO), the fractions of different Ru species in these fresh catalysts can be estimated (Figure S7 and Table S2). It can be calculated that the high-valence ruthenium species (RuO_x + RuO₂) accounted for the percentage of total Ru loading in ϕ -P-Ru/AC-HNO₃ catalyst is the largest (44.4%), followed by the catalysts ϕ -P-Ru/AC-HCl (29.9%), ϕ -P-Ru/AC (20.0%), and the original Ru/AC (10.8%). The high-valence Ru species are reported to be the crucial active ones in Ru-based catalysts for this reaction [24,27]. Therefore, it may be inferred that the substitution of inorganic RuCl₃

precursor by hetero-atomic organometallic complex ϕ -P-Ru in the catalyst could lead to more active species, and the modification of support, especially by nitric acid, could further increase the active species in ϕ -P-Ru catalyst, which is significant to improve the catalysts' catalytic activity. In addition, for the spent catalysts, ϕ -P-Ru/AC-HNO₃ still has the maximum amount of active ruthenium species after the reaction, much higher than that in the other catalysts (Figure 5b).

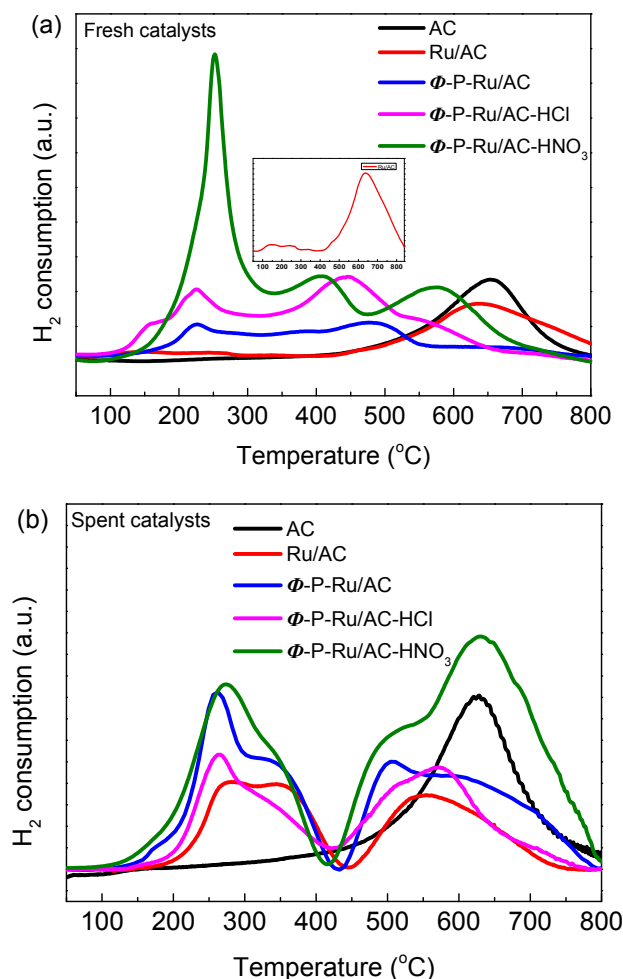


Figure 5. TPR profiles of the fresh (a) and spent (b) Ru-based catalysts.

To further distinguish the valence change of the Ru species and the interactions between the functional groups and active species, the chemical states of Ru were measured by XPS technique. Since the Ru3d signal is overlapped with that of Cls, Ru 3p_{3/2} spectra of the catalysts are recorded and deconvoluted (Figure S8). In contact with the air, ruthenium species can't stably exist in a single form, but in many forms [34]. Therefore, as mentioned in our previous work, the Ru 3p signal in the Ru/AC catalyst can be deconvoluted into four species, corresponding to metallic Ru⁰, RuCl₃, RuO₂ and RuO_x at 461.7, 463.4, 464.6 and 466.1 eV, and the relative content of them is 14.0%, 49.6%, 19.0% and 17.4%, respectively (Table 3) [35–37]. The percentage of Ru species presented in the form of ruthenium oxides (RuO₂ and RuO_x) in the fresh catalysts decreases in the order: ϕ -P-Ru/AC-HNO₃ (53.6%) > ϕ -P-Ru/AC-HCl (48.4%) > ϕ -P-Ru/AC (45.2%) > Ru/AC (36.4%). The amount of active species in the fresh ϕ -P-Ru/AC-HNO₃ is the largest, much higher than that in the original catalyst Ru/AC, which is similar to the TPR results. For the catalysts after the reaction, the relative amount of the oxidized state Ru species reduces, and that of the metallic Ru⁰ increases, indicating that the reduction of high-valence Ru species occurred in the reaction, which can lead to the activity decline of

the Ru-based catalysts [29]. The amount of ruthenium oxides in the spent catalysts also changes in the same order: ϕ -P-Ru/AC-HNO₃ (45.3%) > ϕ -P-Ru/AC-HCl (44.3%) > ϕ -P-Ru/AC (36.9%) > Ru/AC (29.3%). In comparison with the data after the reaction, the relative amount of the active species in ϕ -P-Ru/AC-HNO₃ catalyst is still higher than that of other catalysts after the reaction, which may contribute to its sustaining higher activity after 48 h reaction. In addition, compared with Ru/AC, it can also be seen from the shifts of the binding energy that an enhanced interaction may exist between the modified functional groups on the support and hetero-atomic ϕ -P-Ru species in the prepared organic complex catalysts. Therefore, it can be proved that the substitution of RuCl₃ precursor by ϕ -P-Ru leads to more active species in the catalyst, and the modification of support, especially by nitric acid, generates an enhanced interaction between the modified functional groups on support and active Ru species in ϕ -P-Ru catalyst, which is favorable to further augment the amount of active species, further improving the catalytic performance of the ϕ -P-Ru catalyst.

Table 3. The relative content and binding energy of ruthenium species in the fresh and spent catalysts.

Samples	Binding Energy (eV), (Area%)				(Area%)
	Ru	RuCl ₃	RuO ₂	RuO _x	RuO _x + RuO ₂
Fresh Ru/AC	461.7 (14.0)	463.4 (49.6)	464.6 (19.0)	466.1 (17.4)	(36.4)
Fresh ϕ -P-Ru/AC	461.2 (14.9)	462.8 (37.9)	464.2 (24.5)	465.1 (22.7)	(45.2)
Fresh ϕ -P-Ru/AC-HNO ₃	461.3 (9.9)	463.0 (38.5)	464.4 (34.9)	465.7 (16.7)	(53.6)
Fresh ϕ -P-Ru/AC-HCl	461.9 (12.5)	463.5 (39.1)	464.6 (28.2)	465.7 (20.2)	(48.4)
Spent Ru/AC	461.0 (26.2)	463.0 (44.5)	465.1 (14.6)	466.5 (14.7)	(29.3)
Spent ϕ -P-Ru/AC	461.7 (18.6)	463.1 (44.5)	464.4 (19.8)	465.1 (17.1)	(36.9)
Spent ϕ -P-Ru/AC-HNO ₃	461.3 (19.4)	463.1 (35.3)	464.8 (31.1)	466.3 (14.2)	(45.3)
Spent ϕ -P-Ru/AC-HCl	461.5 (16.2)	463.2 (39.5)	464.2 (27.8)	465.8 (16.5)	(44.3)

2.7. The Adsorption Property of the Synthesized Catalysts for Reactants

In order to study the adsorption capacity of the synthesized catalysts for the reactants, the TPD measurements were conducted and the results are shown in Figure 6. Specifically, the area of the desorption peak reflects the active species amount in the catalyst; the desorption temperature correlates with the adsorption strength of the adsorbed reactants on the catalyst [22]. A desorption peak for C₂H₂ is centered at ca. 400 °C for all the Ru-based catalysts (Figure 6a), and the desorption area for C₂H₂ gradually increases in the order: Ru/AC < ϕ -P-Ru/AC < ϕ -P-Ru/AC-HCl < ϕ -P-Ru/AC-HNO₃. However, the desorption temperature for C₂H₂ increases in a reverse order. This indicates that the substitution of RuCl₃ precursor by ϕ -P-Ru enhances the adsorption capacity of C₂H₂, which is beneficial for the hydrochlorination of acetylene. Notably, the weakly bound species exhibits a lower desorption activation energy and will then undergo the desorption at lower temperatures. Therefore, the shift from the higher desorption temperature of C₂H₂ to lower one may ascribe to the interaction between the hetero-atomic ruthenium organic complex and modified functional groups on the support, resulting in different C₂H₂ chemisorption strengths [34]. The weakly bound acetylene is also beneficial for the reaction to inhibit the coking deposition on the catalysts. In contrast, the peaks of HCl desorption are broad bands located in the range of 200–800 °C for the fresh samples, suggesting the presence of the multi-status adsorbed HCl. The area of HCl desorption peak also gradually increases in the order: Ru/AC < ϕ -P-Ru/AC < ϕ -P-Ru/AC-HCl < ϕ -P-Ru/AC-HNO₃. Moreover, the desorption temperatures of HCl in the ϕ -P-Ru-based catalysts are much higher than that in Ru/AC. These indicate that the ϕ -P-Ru-based catalysts exhibit the superior adsorption capacity and strength of HCl to those of the original Ru/AC catalyst. In general, it can be inferred that the substitution of original RuCl₃ by hetero-atomic ϕ -P-Ru organic species strengthens the adsorption capacity of reactants, moreover, the treatment of support, especially by nitric acid, in ϕ -P-Ru catalysts, could produce an enhanced interaction between the hetero-atomic ϕ -P-Ru species and support to further enhance the adsorption ability for reactants, improving the activity of the catalyst.

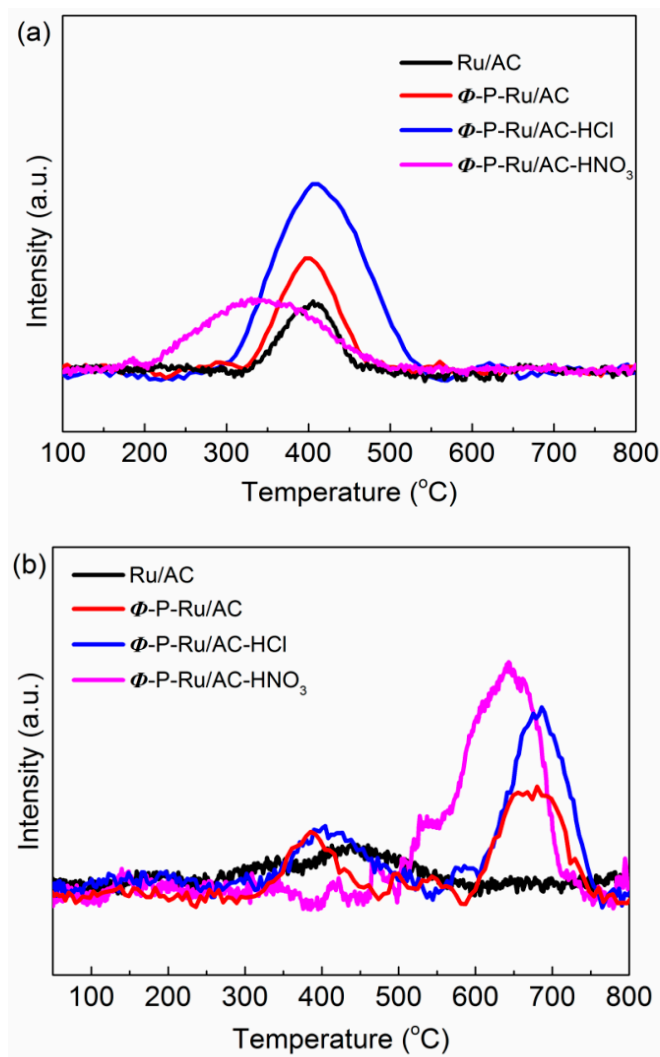


Figure 6. C₂H₂- (a) and HCl- (b) TPD profiles of the fresh Ru-based catalysts.

2.8. The Reusability of the Catalyst with 0.1% Ru Loading

In fact, the ruthenium catalyst with low metal loading (0.1 wt% Ru) has better activity than that with high metal loading (1.0 wt%), but it can't be accurately characterized due to its low metal content [19]. To investigate the reusability of catalyst, the spent ϕ -P-Ru/AC-HNO₃ (0.1 wt% Ru, 2 mL) was transferred to a beaker, then 20 mL HNO₃ (5 mol·L⁻¹) solution was added; the catalyst was placed at room temperature for 6 h under stirring, then it was filtered and washed to pH = 7 with distilled water, followed by desiccation at 140 °C for 24 h. The yield catalyst was reused to catalyze the reaction for another 48 h. Figure 7 shows the reusability of the catalyst. A stable acetylene conversion of 99.2% could be achieved over the catalyst in the first run. Compared with the ruthenium-based catalysts reported in the literatures, it also has a considerable activity (Table S3). After recycling 5 times, the conversion of acetylene was still able to be stabilized at 92.5%.

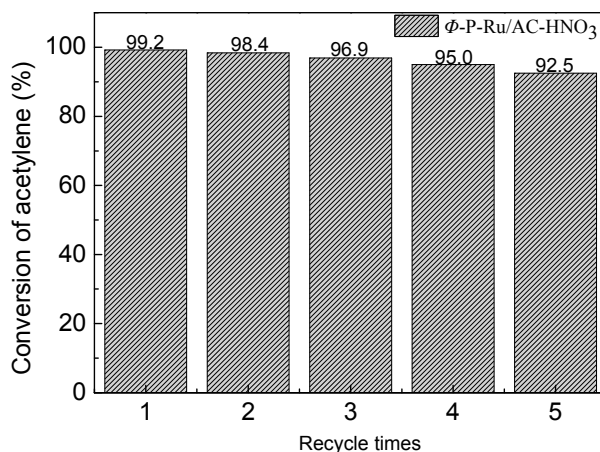


Figure 7. Catalytic performance of the recycled ϕ -P-Ru/AC-HNO₃ catalysts. Reaction conditions: temperature (T) = 180 °C, GHSV (C₂H₂) = 180 h⁻¹ and V_{HCl}/V_{C₂H₂} = 1.15.

3. Experimental

3.1. Chemicals and Catalyst Preparation

Ruthenium chloride (Ru content \geq 48.7%), hydrochloric acid, nitric acid (65.0–68.0 wt%) and tri-(triphenylphosphine) ruthenium dichloride (purity \geq 97%) were purchased from Alfa Aesar Chemical Co., Ltd. (Shanghai, China), and used without further purification. The coconut AC was purchased from S. S. Activated Carbon Industry Science and Technology Co., Ltd. (Nanping, China). The modification of AC was carried out according to the previous method with 5 mol·L⁻¹ nitric acid or 12 mol·L⁻¹ hydrochloric acid [38–40], and the resulted samples were denoted as AC-HNO₃ or AC-HCl. Ru catalysts were synthesized by a wetness impregnation method [17,29]. For the synthesis of tris(triphenylphosphine) ruthenium dichloride catalyst, 0.324 g of tris-(triphenylphosphine) ruthenium dichloride was accurately weighed and dissolved in 300 mL of ethanol, followed by the addition of 3 g of AC. The mixture was stirred at ambient temperature for 24 h, and then adjusted the temperature to 40 °C with a rotary evaporator to remove ethanol, finally the solid residue was held at 140 °C for 24 h to obtain the catalyst, which was named ϕ -P-Ru/AC. For comparison, the Ru/AC catalyst was also synthesized by quantitatively impregnating 3 g AC with 6.4 mL RuCl₃ ethanol solution (0.01 g mL⁻¹), then the mixture was dipped while stirring for a whole day at ambient temperature. Subsequently, the resultant sample was desiccated at 140 °C for a day to obtain the catalyst. In the same way, the carrier was substituted by the acidification pretreated AC, and ϕ -P-Ru/AC-HNO₃ and ϕ -P-Ru/AC-HCl catalysts were obtained. Ru-P(Cy)₃/AC catalyst was also prepared by complexing aliphatic phosphine (P(Cy)₃, Cy = cyclohexyl) ligand with RuCl₃ precursor (Ru:P(Cy)₃ = 1:1, molar ratio). The loading of Ru in Ru catalysts was all calculated as 1.0 wt%.

3.2. Catalyst Characterization

The fourier transform infrared spectroscopy (FT-IR) spectra of the catalysts were obtained by a Nicolet NEXUS 470 FT-IR spectrometer (Thermo Fisher Scientific, Waltham, MA, USA) to distinguish the functional groups information on the surface; the catalyst is ground into powder and evenly mixed with potassium bromide in a certain proportion during the preparation process, and the pellet is formed. Low-temperature N₂ physical adsorption-desorption at -196 °C were conducted by a Micromeritics ASAP 2020 instrument (Micromeritics Instrument Ltd., Atlanta, GA, USA) to measure the texture physical properties of the samples, prior to the test, the catalysts need to be degassed at 150 °C for 6 h. Inductively coupled plasma-atomic emission spectrometry (ICP-AES) was utilized by a Varian 725-ES instrument (Varian, Palo Alto, CA, USA) to evaluate the absolute content of Ru in catalysts, prior to the test, the samples need to be digested by aqua regia solution.

Thermogravimetric analysis (TGA) was performed by a METTLER TOLEDO TGA/DSC 2 analyzer (METTLER TOLEDO, Zurich, Switzerland) under a $30 \text{ mL}\cdot\text{min}^{-1}$ air flow, and the sample was heated from 25 to 800 °C with an increment of $10 \text{ }^\circ\text{C}\cdot\text{min}^{-1}$ to assess the coking deposition on the spent catalysts. X-ray diffraction (XRD) patterns of the catalysts were obtained by a D8 Advance Bruker diffractometer (Bruker, Karlsruhe, Germany) at the wide angles ($10\text{--}90^\circ$ in 2θ) to indirectly elucidate the dispersion of the Ru species. Transmission electron microscopy (TEM) experiments were conducted with a JEM2010 electron microscope instrument (JEOL Ltd., Tokyo, Japan), before the images were obtained, the sample powders need to be firstly dispersed in absolute ethanol and then supported on copper grids to obtain the images. H_2 Temperature-programmed reduction (H_2 -TPR) profiles were obtained by a ChemBET PulsarTM TPD/TPR instrument (Quantachrome, Boynton Beach, FL, USA); prior to each test, 100 mg sample was treated with high-purity N_2 gas at 100 °C for 1 h; after being cooled, the sample was heated from 30 to 800 °C with a rate of $10 \text{ }^\circ\text{C}\cdot\text{min}^{-1}$ under $40 \text{ mL}\cdot\text{min}^{-1}$ flow of 10.0% H_2/Ar . X-ray photoelectron spectroscopy (XPS) was performed on an Axis Ultra spectrometer (Shimadzu, Kyoto, Japan); the spectral regions of Ru 3p and C 1s levels were recorded for each sample. The spectra were calibrated with the C1s peak (284.6 eV). Temperature-programmed desorption (TPD) profiles were obtained by a ChemBET PulsarTM TPD/TPR instrument (Quantachrome, Boynton Beach, FL, USA); 100 mg sample was placed in a C_2H_2 or HCl flow at 180 °C for 6 h; then, C_2H_2 -TPD or HCl-TPD profiles were recorded as the sample was heated from room temperature to 800 °C with a rate of $10 \text{ }^\circ\text{C}\cdot\text{min}^{-1}$ under a N_2 flow of $45 \text{ mL}\cdot\text{min}^{-1}$.

3.3. Catalytic Performance Test

The catalytic performance test was carried out in a steel reactor (i.d. of 10 mm). A $20 \text{ mL}\cdot\text{min}^{-1}$ N_2 was flowed through the whole pipeline to remove the water vapor and other moisture. Then, a HCl flow of $20 \text{ mL}\cdot\text{min}^{-1}$ was then passed through the bed to activate the 2 mL filled catalyst. When the reaction began, C_2H_2 ($6 \text{ mL}\cdot\text{min}^{-1}$) and HCl ($6.9 \text{ mL}\cdot\text{min}^{-1}$) continuous flows controlled via mass flow controllers were passed through the heated reactor under atmospheric pressure. $V_{\text{HCl}}/V_{\text{C}_2\text{H}_2}$ and $\text{GHSV}(\text{C}_2\text{H}_2)$ were maintained at 1.15 and 180 h^{-1} , respectively. The gas products were analyzed in situ with a Shimadzu gas chromatography (GC-2014C).

4. Conclusions

Carbon-supported Ru-based catalysts were synthesized for the direct synthesis of VCM, and the effects of the hetero-atomic ruthenium precursor and modification of the support on the reaction were also studied in detail. The results of performance test elucidate that the superior performance can be reached over ϕ -P-Ru/AC- HNO_3 catalyst, with a more slowly decline of conversion from the initial 97.2% to 87.0% within 48 h, and there is a relative increment of 87.0% in acetylene conversion compared with the original catalyst Ru/AC. The characterization results of FT-IR, BET, ICP-AES, TGA, XRD, TEM, TPR, XPS, and TPD reveal that the substitution of original RuCl_3 inorganic precursor by the hetero-atomic ϕ -P-Ru organic species in the catalysts results in more amount of active species; the treatment of support in ϕ -P-Ru/AC catalysts could produce an enhanced interaction between the modified functional groups on the support and hetero-atomic ϕ -P-Ru organic species. The enhanced interaction is favorable to anchor and further reduce the loss of Ru species during the reaction, greatly strengthens the adsorption ability of C_2H_2 and HCl reactants, and further augment the amount of active components in the catalysts, thereby improving the activity and stability of the resultant catalysts. However, the treatment of support by acid leads to more carbon deposition, which is unfavorable for the catalysis of the reaction, and this needs to be improved in the future studies. In brief, the obtained results can also provide an effective strategy to explore the economic and environmentally benign mercury-free catalysts for acetylene hydrochlorination.

Supplementary Materials: The following are available online at <http://www.mdpi.com/2073-4344/8/7/276/s1>, Table S1: Ru content in the fresh and used Ru-based catalysts, based on the ICP analysis, Table S2: The Ru species accounted for the percentage of total Ru loading in each fresh catalyst, determined by TPR profiles,

Table S3: Comparative study for the catalytic efficiency of this catalytic system over the literature reported ruthenium-based catalysts, Figure S1: The acetylene conversion (a) and selectivity to VCM (b) over the supports, Figure S2: The acetylene conversion of the Ru-P(Cy)₃/AC catalyst, Figure S3: FT-IR spectra of the supports: (a) AC, (b) AC-HNO₃, (c) AC-HCl, Figure S4: Nitrogen adsorption-desorption isotherms of the fresh (a) and spent (b) catalysts, Figure S5: Thermogravimetric analysis (TGA) curves of fresh and spent catalysts recorded in air atmosphere, Figure S6: Particle size distribution of Ru-based catalysts, Figure S7: The deconvoluted H₂-TPR profiles of the fresh catalysts: (a) Ru/AC, (b) ϕ -P-Ru/AC, (c) ϕ -P-Ru/AC-HCl, (d) ϕ -P-Ru/AC-HNO₃, Figure S8: High-resolution XPS spectra of Ru 3p for the fresh and spent catalysts, Figure S9: The activity of the catalyst regenerated by HCl and nitric acid.

Author Contributions: H.Z. and J.Z. conceived and designed the experiments; X.L. performed the experiments; X.L., B.M., C.Z. and H.D. analyzed the data; B.D. contributed reagents/materials/analysis tools; H.Z. and X.L. wrote the paper.

Acknowledgments: This project is supported by National Natural Science Foundation of China (Grant No. 21706167, 21776179), Fok Ying Tung Education Foundation (No. 161108), the Program for Changjiang Scholars and Innovative Research Team in University (No. IRT_15R46), Yangtze River Scholar Research Project of Shihezi University (No. CJXZ201601), and the Start-Up Foundation for Young Scientists of Shihezi University (RCZX201507).

Conflicts of Interest: The authors declare no conflict of interest.

References

1. Hutchings, G.J. Vapor phase hydrochlorination of acetylene: Correlation of catalytic activity of supported metal chloride catalysts. *J. Catal.* **1985**, *96*, 292–295. [[CrossRef](#)]
2. Li, X.; Zhu, M.; Dai, B. AuCl₃ on polypyrrole-modified carbon nanotubes as acetylene hydrochlorination catalysts. *Appl. Catal. B-Environ.* **2013**, *142–143*, 234–240. [[CrossRef](#)]
3. Wang, B.; Yu, L.; Zhang, J.; Pu, Y.; Zhang, H.; Li, W. Phosphorus-doped carbon supports enhance gold-based catalysts for acetylene hydrochlorination. *RSC Adv.* **2014**, *4*, 15877–15885. [[CrossRef](#)]
4. Enache, D.I.; Edwards, J.K.; Landon, P.; Solsonaespriu, B.; Carley, A.F.; Herzing, A.A.; Watanabe, M.; Kiely, C.J.; Knight, D.W.; Hutchings, G.J. Solvent-free oxidation of primary alcohols to aldehydes using Au-Pd/TiO₂ catalysts. *Science* **2006**, *311*, 362–365. [[CrossRef](#)] [[PubMed](#)]
5. Malta, G.; Freakley, S.J.; Kondrat, S.A.; Hutchings, G.J. Acetylene hydrochlorination using Au/carbon: A journey towards single site catalysis. *Chem. Commun.* **2017**, *53*, 11733–11746. [[CrossRef](#)] [[PubMed](#)]
6. Zhang, H.; Li, W.; Li, X.; Zhao, W.; Gu, J.; Qi, X.; Dong, Y.; Dai, B.; Zhang, J. Non-mercury catalytic acetylene hydrochlorination over bimetallic Au-Ba(II)/AC catalysts. *Catal. Sci. Technol.* **2015**, *5*, 1870–1877. [[CrossRef](#)]
7. Zhou, K.; Wang, W.; Zhao, Z.; Luo, G.; Miller, J.T.; Wong, M.S.; Wei, F. Synergistic gold–bismuth catalysis for non-mercury hydrochlorination of acetylene to vinyl chloride monomer. *ACS Catal.* **2014**, *4*, 3112–3116. [[CrossRef](#)]
8. Zhao, J.; Xu, J.; Xu, J.; Ni, J.; Zhang, T.; Xu, X.; Li, X. Activated-carbon-supported gold-cesium(I) as highly effective catalysts for hydrochlorination of acetylene to vinyl chloride. *ChemPlusChem* **2014**, *80*, 196–201. [[CrossRef](#)]
9. Zhao, J.; Xu, J.; Xu, J.; Zhang, T.; Di, X.; Ni, J.; Li, X. Enhancement of Au/AC acetylene hydrochlorination catalyst activity and stability via nitrogen-modified activated carbon support. *Chem. Eng. J.* **2015**, *262*, 1152–1160. [[CrossRef](#)]
10. Zhou, K.; Jia, J.; Li, C.; Xu, H.; Zhao, J.; Luo, G.; Wei, F. A low content Au-based catalyst for hydrochlorination of C₂H₂ and its industrial scale-up for future PVC processes. *Green Chem.* **2014**, *17*, 356–364. [[CrossRef](#)]
11. Wang, L.; Shen, B.; Zhao, J.; Bi, X. Trimetallic Au-Cu-K/AC for acetylene hydrochlorination. *Can. J. Chem. Eng.* **2017**, *95*, 1069–1075. [[CrossRef](#)]
12. Wang, S.; Shen, B.; Song, Q. Kinetics of acetylene hydrochlorination over bimetallic Au-Cu/C catalyst. *Catal. Lett.* **2010**, *134*, 102–109. [[CrossRef](#)]
13. Chao, S.; Guan, Q.; Li, W. Study of the active site for acetylene hydrochlorination in AuCl₃/C catalysts. *J. Catal.* **2015**, *330*, 273–279. [[CrossRef](#)]
14. Wan, F.; Chao, S.; Guan, Q.; Wang, G.; Li, W. Reaction mechanisms of acetylene hydrochlorination catalyzed by AuCl₃/C catalysts: A density functional study. *Catal. Commun.* **2017**, *101*, 120–124. [[CrossRef](#)]
15. Johnston, P.; Carthey, N.; Hutchings, G.J. Discovery, development, and commercialization of gold catalysts for acetylene hydrochlorination. *J. Am. Chem. Soc.* **2015**, *137*, 14548–14557. [[CrossRef](#)] [[PubMed](#)]

16. Zhu, M.; Kang, L.; Su, Y.; Zhang, S.; Dai, B. MCl_x (M = Hg, Au, Ru; x = 2, 3) catalyzed hydrochlorination of acetylene—A density functional theory study. *Can. J. Chem.* **2013**, *91*, 120–125. [[CrossRef](#)]
17. Zhang, J.; Sheng, W.; Guo, C.; Li, W. Acetylene hydrochlorination over bimetallic Ru-based catalysts. *RSC Adv.* **2013**, *3*, 21062–21068. [[CrossRef](#)]
18. Jin, Y.; Li, G.; Zhang, J.; Pu, Y.; Li, W. Effects of potassium additive on the activity of Ru catalyst for acetylene hydrochlorination. *RSC Adv.* **2015**, *5*, 37774–37779. [[CrossRef](#)]
19. Zhang, H.; Li, W.; Jin, Y.; Sheng, W.; Hu, M.; Wang, X.; Zhang, J. Ru-Co(III)-Cu(II)/SAC catalyst for acetylene hydrochlorination. *Appl. Catal. B-Environ.* **2016**, *189*, 56–64. [[CrossRef](#)]
20. Gu, J.; Gao, Y.; Zhang, J.; Li, W.; Dong, Y.; Han, Y. Hydrochlorination of acetylene catalyzed by an activated carbon-supported ammonium hexachlororuthenate complex. *Catalysts* **2017**, *7*, 17. [[CrossRef](#)]
21. Shang, S.; Zhao, W.; Wang, Y.; Li, X.; Zhang, J.; Han, Y.; Li, W. Highly efficient Ru@IL/AC to substitute mercuric catalyst for acetylene hydrochlorination. *ACS Catal.* **2017**, *7*, 3510–3520. [[CrossRef](#)]
22. Man, B.; Zhang, H.; Zhang, J.; Li, X.; Xu, N.; Dai, H.; Zhu, M.; Dai, B. Oxidation modification of Ru-based catalyst for acetylene hydrochlorination. *RSC Adv.* **2017**, *7*, 23742–23750. [[CrossRef](#)]
23. Wang, X.; Dai, B.; Wang, Y.; Yu, F. Nitrogen-doped pitch-based spherical active carbon as a nonmetal catalyst for acetylene hydrochlorination. *ChemCatChem* **2014**, *6*, 2339–2344. [[CrossRef](#)]
24. Zhong, J.; Xu, Y.; Liu, Z. Heterogeneous non-mercury catalysts for acetylene hydrochlorination: Progress, Challenges, and Opportunities. *Green Chem.* **2018**, *20*, 2412–2427. [[CrossRef](#)]
25. Li, X.; Zhang, H.; Man, B.; Hou, L.; Zhang, C.; Dai, H.; Zhu, M.; Dai, B.; Dong, Y.; Zhang, J. Activated carbon-supported tetrapropylammonium perruthenate catalysts for acetylene hydrochlorination. *Catalysts* **2017**, *7*, 311. [[CrossRef](#)]
26. Biniak, S.; Szymański, G.; Siedlewski, J.; Tkowski, A.Ś.J. The characterization of activated carbons with oxygen and nitrogen surface groups. *Carbon* **1997**, *35*, 1799–1810. [[CrossRef](#)]
27. Nyquist, R.A.; Potts, W.J. Infrared absorptions characteristic of the terminal acetylenic group (–C≡C–H). *Spectrochim. Acta* **1960**, *16*, 419–427. [[CrossRef](#)]
28. Pu, Y.; Zhang, J.; Yu, L.; Jin, Y.; Li, W. Active ruthenium species in acetylene hydrochlorination. *Appl. Catal. A-Gen.* **2014**, *488*, 28–36. [[CrossRef](#)]
29. Nkosi, B.; Coville, N.J.; Hutchings, G.J.; Adams, M.D.; Friedl, J.; Wagner, F.E. Hydrochlorination of acetylene using gold catalysts: A study of catalyst deactivation. *J. Catal.* **1991**, *128*, 366–377. [[CrossRef](#)]
30. Zhang, H.; Dai, B.; Wang, X.; Li, W.; Han, Y.; Gu, J.; Zhang, J. Non-mercury catalytic acetylene hydrochlorination over bimetallic Au–Co(III)/SAC catalysts for vinyl chloride monomer production. *Green Chem.* **2013**, *15*, 829–836. [[CrossRef](#)]
31. Liu, F.G.; Du, M.; Zhang, J.; Qiu, M. Electrochemical behavior of Q235 steel in saltwater saturated with carbon dioxide based on new imidazoline derivative inhibitor. *Corros. Sci.* **2009**, *51*, 102–109. [[CrossRef](#)]
32. Gao, P.; Wang, A.; Wang, X.; Zhang, T. Synthesis and catalytic performance of highly ordered Ru-containing mesoporous carbons for hydrogenation of cinnamaldehyde. *Catal. Lett.* **2008**, *125*, 289–295. [[CrossRef](#)]
33. Zgolicz, P.D.; Stassi, J.P.; Yañez, M.J.; Scelza, O.A.; Miguel, S.R.D. Influence of the support and the preparation methods on the performance in citral hydrogenation of Pt-based catalysts supported on carbon nanotubes. *J. Catal.* **2012**, *290*, 37–54. [[CrossRef](#)]
34. Man, B.; Zhang, H.; Zhang, C.; Li, X.; Dai, H.; Zhu, M.; Dai, B.; Zhang, J. Effect of Ru/Cl ratio on the reaction of acetylene hydrochlorination. *New J. Chem.* **2017**, *41*, 23–49. [[CrossRef](#)]
35. Fuente, J.L.; Martínez-Huerta, M.V.; Rojas, S.; Hernández-Fernández, P.; Terreros, P.; Fierro, J.L.; Peña, M.A. Tailoring and structure of PtRu nanoparticles supported on functionalized carbon for DMFC applications: New evidence of the hydrous ruthenium oxide phase. *Appl. Catal. B-Environ.* **2009**, *88*, 505–514. [[CrossRef](#)]
36. Suñol, J.J.; Bonneau, M.E.; Roué, L.; Guay, D.; Schulz, R. XPS surface study of nanocrystalline Ti-Ru-Fe materials. *Appl. Surf. Sci.* **2000**, *158*, 252–262. [[CrossRef](#)]
37. Chan, H.Y.; Takoudis, C.G.; Weaver, M.J. High-pressure oxidation of ruthenium as probed by surface-enhanced Raman and X-ray photoelectron spectroscopies. *J. Catal.* **1997**, *172*, 336–345. [[CrossRef](#)]
38. Ke, J.; Zhao, Y.; Yin, Y.; Chen, K.; Duan, X.; Ye, L.; Yuan, Y. Yttrium chloride-modified Au/AC catalysts for acetylene hydrochlorination with improved activity and stability. *J. Rare Earth* **2017**, *35*, 1083–1091. [[CrossRef](#)]

39. Cao, H.; Xing, L.; Wu, G.; Xie, Y.; Shi, S.; Zhang, Y.; Minakata, D.; Crittenden, J.C. Promoting effect of nitration modification on activated carbon in the catalytic ozonation of oxalic acid. *Appl. Catal. B-Environ.* **2014**, *146*, 169–176. [[CrossRef](#)]
40. Conte, M.; Davies, C.J.; Morgan, D.J.; Davies, T.E.; Carley, A.F.; Johnston, P.; Hutchings, G.J. Modifications of the metal and support during the deactivation and regeneration of Au/C catalysts for the hydrochlorination of acetylene. *Catal. Sci. Technol.* **2013**, *3*, 128–134. [[CrossRef](#)]



© 2018 by the authors. Licensee MDPI, Basel, Switzerland. This article is an open access article distributed under the terms and conditions of the Creative Commons Attribution (CC BY) license (<http://creativecommons.org/licenses/by/4.0/>).